HHS Public Access

Author manuscript

JAMA Neurol. Author manuscript; available in PMC 2016 July 11.

Published in final edited form as:

JAMA Neurol. 2014 October ; 71(10): 1266–1274. doi:10.1001/jamaneurol.2014.1638.

Structural Growth Trajectories and Rates of Change in the First 3 Months of Infant Brain Development

Dominic Holland, PhD, **Linda Chang, MD**, **Thomas M. Ernst, PhD**, **Megan Curran**, **Steven D. Buchthal, PhD**, **Daniel Alicata, MD**, **Jon Skranes, MD**, **Heather Johansen**, **Antonette Hernandez**, **Robyn Yamakawa**, **Joshua M. Kuperman, PhD**, and **Anders M. Dale, PhD**

Department of Neurosciences, University of California, San Diego, La Jolla (Holland, Dale); Multimodal Imaging Laboratory, University of California, San Diego, La Jolla (Holland, Curran, Kuperman, Dale); Department of Medicine, John A. Burns School of Medicine, University of Hawaii, Honolulu (Chang, Ernst, Buchthal, Alicata, Skranes, Johansen, Hernandez, Yamakawa); Department of Laboratory Medicine, Children's and Women's Health, Norwegian University of Science and Technology, Trondheim, Norway (Skranes); Department of Radiology, University of California, San Diego, La Jolla (Kuperman, Dale)

Abstract

IMPORTANCE—The very early postnatal period witnesses extraordinary rates of growth, but structural brain development in this period has largely not been explored longitudinally. Such assessment may be key in detecting and treating the earliest signs of neurodevelopmental disorders.

OBJECTIVE—To assess structural growth trajectories and rates of change in the whole brain and regions of interest in infants during the first 3 months after birth.

Corresponding Author: Dominic Holland, PhD, Multimodal Imaging Laboratory and Department of Neurosciences, University of California, San Diego, 8950 Villa La Jolla Dr, Ste C101, La Jolla, CA 92037 (dominic.holland@gmail.com).

Supplemental content at jamaneurology.com

Author Contributions: Dr Holland had full access to all of the data in the study and takes responsibility for the integrity of the data and the accuracy of the data analysis.
Study concept and design: Holland, Chang, Ernst, Dale.
Acquisition, analysis, or interpretation of data: Holland, Ernst, Curran, Buchthal, Alicata, Skranes, Johansen, Hernandez, Yamakawa, Kuperman, Dale.
Drafting of the manuscript: Holland, Chang.
Critical revision of the manuscript for important intellectual content: All authors.
Statistical analysis: Holland, Dale.
Obtained funding: Chang, Ernst, Dale.
Administrative, technical, or material support: Holland, Chang, Ernst, Kuperman, Dale.
Study supervision: Holland, Chang, Ernst, Buchthal, Skranes, Dale.

Conflict of Interest Disclosures: Dr Dale is a founder and holds equity in CorTechs Labs, Inc, and also serves on its Scientific Advisory Board. The terms of this arrangement have been reviewed and approved by the University of California, San Diego, in accordance with its conflict of interest policies. No other disclosures were reported.

Additional Contributions: We thank the children and parents who volunteered to participate in this study; our clinical research staff, Christine Cloak, PhD, Lynn Anderson, BA, and Krista Bridges, RN, and our MR technician, Eric Cunningham, BS, at John A. Burns School of Medicine, University of Hawaii; and our image processing staff, Yoonho Chung, BS, and Matt Erhart, BS, at the University of California, San Diego. We are also grateful to Terry Jernigan, PhD, and Linda McEvoy, PhD, the University of California, San Diego, for invaluable discussions regarding the results and the writing of the manuscript.

DESIGN, SETTING, AND PARTICIPANTS—Serial structural T1-weighted and/or T2-weighted magnetic resonance images were obtained for 211 time points from 87 healthy term-born or term-equivalent preterm-born infants, aged 2 to 90 days, between October 5, 2007, and June 12, 2013.

MAIN OUTCOMES AND MEASURES—We segmented whole-brain and multiple subcortical regions of interest using a novel application of Bayesian-based methods. We modeled growth and rate of growth trajectories nonparametrically and assessed left-right asymmetries and sexual dimorphisms.

RESULTS—Whole-brain volume at birth was approximately one-third of healthy elderly brain volume, and did not differ significantly between male and female infants (347 388 mm^3 and 335 509 mm^3, respectively, $P = .12$). The growth rate was approximately 1%/d, slowing to 0.4%/d by the end of the first 3 months, when the brain reached just more than half of elderly adult brain volume. Overall growth in the first 90 days was 64%. There was a significant age-by-sex effect leading to widening separation in brain sizes with age between male and female infants (with male infants growing faster than females by 200.4 mm^3/d, SE = 67.2, $P = .003$). Longer gestation was associated with larger brain size (2215 mm^3/d, SE = 284, $P = 4\times10^{-13}$). The expected brain size of an infant born one week earlier than average was 5% smaller than average; at 90 days it will not have caught up, being 2% smaller than average. The cerebellum grew at the highest rate, more than doubling in 90 days, and the hippocampus grew at the slowest rate, increasing by 47% in 90 days. There was left-right asymmetry in multiple regions of interest, particularly the lateral ventricles where the left was larger than the right by 462 mm^3 on average (approximately 5% of lateral ventricular volume at 2 months). We calculated volume-by-age percentile plots for assessing individual development.

CONCLUSIONS AND RELEVANCE—Normative trajectories for early postnatal brain structural development can be determined from magnetic resonance imaging and could be used to improve the detection of deviant maturational patterns indicative of neurodevelopmental disorders.

There is a lack of quantitative in vivo studies of early postnatal brain development, particularly longitudinal studies, in healthy term infants. Most published studies are cross-sectional and focus on the effects in infants of being born preterm.[1–4] There remains therefore a serious gap in our knowledge of the normally maturing brain,[5] because the earliest periods of postnatal development are the most dynamic[6] and may have pronounced bearing on neurodevelopmental disorders, particularly those eventually manifesting as childhood-onset neuropsychiatric disorders (eIntroduction in the Supplement). Thus, it is important to understand and quantify normal developmental trajectories from which to assess, as early and precisely as possible, deviant maturation patterns indicative of such disorders. In addition, trajectories for subregional brain growth would provide a foundation to correlate the very rapid brain development with concomitant development of cognitive and motor abilities.

The standard clinical approach to assessing structural development of the brain in neonates, measurement of head circumference with a tape, dates back more than 200 years.[7–10] In cases of suspected abnormalities, computed tomography[11] has been used to visualize the brain in vivo, but it uses ionizing x-rays.[12] Magnetic resonance (MR) imaging (MRI) does

not involve harmful radiation, and it provides a rich set of contrasts for visualizing different types of tissue.[13] In particular, T1-weighted and T2-weighted imaging allows quantitative assessment of brain structure and can be performed repeatedly for longitudinal evaluations without deleterious effects.

Reasons for the scarcity of MRI developmental studies to date include the practical difficulties in enrolling and imaging infants in the days and weeks immediately after birth, and difficulties in image postprocessing and analysis.[13] In addition to the usual issues that affect precision in quantitative image analysis in adults, such as geometric distortion due to nonlinearity in the main magnetic field of the scanner and nonuniform intensity due to spatial variability in penetration and strength of the radiofrequency excitation pulse, there are other difficulties in analyzing neonatal images, which are typically more pronounced. These include image degradation due to subject motion, often to the point that images are unusable; dramatic changes in head size during the first months of life; very different head shapes arising from natural birth and cesarean delivery; rapid changes in tissue contrast caused by differential myelination across brain regions, decreases in water content,[14] and increases in tissue density, such that on T1-weighted images gray matter, initially brighter than white matter, becomes darker than white matter; low contrast-to-noise ratio between gray and white matter; and resolution difficulties arising from the fact that essentially the full adult folding complexity[15,16] is contained in a third of the adult intracranial volume. As a result of these challenges, direct, automatic, and independent subcortical tissue segmentation of individual neonatal brain images has often proved difficult,[6,17,18] despite recent advances in delineation of myelinated/unmyelinated tissue segmentation in images of infants.[19–21]

In this study, we used a novel application of Bayesian-based methods, described below, to automatically segment neonatal brain structures based on T1-weighted and T2- weighted structural MRI. We present results from what is to our knowledge the largest longitudinal study to date (211 time points from 87 subjects) of cerebral structural development focusing on the first 3 months of postnatal life in healthy term-born or term-equivalent preterm-born infants. We examined multiple regions of interest (ROIs), including lateral ventricles, hippocampus, caudate, and putamen; assessed sexual dimorphisms, left-right asymmetries, and growth rates as a function of age; and calculated sex-specific volume-by-age percentile plots for the brain parenchyma and several subcortical brain regions.

Methods

Participant Enrollment and Study Criteria

A total of 572 parents were screened initially by telephone or at the local hospital and clinics; 180 parents or legal guardians signed a written informed consent, and the study was approved by the institutional review board at the University of Hawaii. After detailed interviews with the parents or legal guardians regarding the mothers' medical and drug use histories, 87 healthy neonates (39 male and 48 female) fulfilling study criteria were enrolled for the current MRI study (Table 1). Images were obtained between October 5, 2007, and June 12, 2013. The majority of infants were mixed race (54%), and the rest were white (non-

Hispanic, 8%), Native Hawaiian/Pacific Islander (22%), Asian (13%), or black (1%). See the eMethods in the Supplement for further details.

Image Acquisition

T1-weighted and T2-weighted MR images were acquired with 3-dimensional pulse sequences on a Siemens TrioTim 3.0-T scanner (Siemens Medical Systems) while the infant slept without sedation (eMethods in the Supplement).

Tissue Segmentation

To perform automatic segmentation on an anatomical image, probabilistic information—spatial prior probabilities for ROIs and likelihoods of intensities given a tissue type—must first be gathered using manually segmented images, a process that is facilitated by mapping the images to an atlas space. Image alignment, nonlinear registration, and correction of intensity non-uniformity were performed using a modified version of Quarc[22,23] (quantitative anatomical regional change), a recently developed method from the Multimodal Imaging Laboratory, University of California, San Diego.

For any given pair of aligned T1 and T2 brain images, the inverse mapping of these images to the atlas can be applied to the spatial prior probability distributions, which, along with both T1 and T2 signal intensities, can be used to assign tissue labels to voxels in the original images. In principle, tissue segmentation will be more precise if multiple modalities with different contrast properties are used, especially if tissue image definition depends on both ROI and modality (see eMethods in the Supplement for further details). Estimates for absolute structure volumes (with standard errors of the mean) are shown in eFigure 1A in the Supplement and numerical values are provided in the eResults and eTable 1 in the Supplement. Figure 1A shows coronal, axial, and sagittal sections of the T1 and T2 atlas images, and Figure 1B shows automatic segmentation (coronal, axial, and sagittal sections) in images from 2 male infants that were not manually segmented.

Growth Trajectory Analysis

Generalized additive mixed model (GAMM)[24] analyses with robust estimation were used to assess growth trajectories from longitudinal measures of structure size. This approach does not enforce a presupposed parametric trajectory (eg, linear or quadratic) but finds a best-fit trajectory (the function $f(t_{ij})$ below), taking into account both the cross-sectional and longitudinal nature of the data. For a given ROI, let Y_{ij} denote the structure size (mean of left and right for bilateral structures) for subject i at time point j, and let t_{ij} denote the subject's age (from birth, measured in days) at that time point. Y_{ij} is modeled as

$$Y_{ij}=f(t_{ij})+g_{o}G_{i}+s_{o}S_{i}+g_{t}G_{i}t_{ij}+s_{t}S_{i}t_{ij}+\varepsilon_{ij}.$$

Here $f(t_{ij})$ is a GAMM "smooth" functional fit to be determined, and the 2 covariates are the subject's mean-centered gestational age at birth[25] G_i (in days) and the subject's sex S_i (male = 0; female = 1). The model parameters to be determined are the coefficients g_0 and s_0 for the offsets in structure size (intercept) arising from effects due to gestational age at birth and sex, and g_t and s_t for age × (gestational age at birth) and age × sex interactions. The term ε_{ij}

is the within-participant error, assumed to be independent and identically normally distributed with zero mean and variance σ_ε^2 (also to be fit by the model). All calculations were carried out in R (version 2.15.0) and MATLAB (version 8.0.0.783; MathWorks) software. In addition, analyses were performed controlling for head circumference or body length at birth in the 63 infants with these data available, by including a term $c_0 C_i$ for subject i, wherein C_i is the mean-centered measure at birth for subject i and c_0 is a cohort coefficient to be determined (eMethods in the Supplement).

Rate of Growth Analysis

Rates of growth for the ROIs were estimated in 2 ways: (1) from the gradient (first derivative with respect to age) of the GAMM-fit curve for the growth trajectory and (2) by taking the strictly longitudinal data, calculating the linear growth rate at the midpoint for each sequential pair of data points for each subject, and then performing a GAMM fit to those estimated growth rate data points.

Volume-for-Age Percentile Plots

We calculated residuals for ROI volume for each time point relative to the respective male or female best-fit growth trajectory from the Equation, and we fit the squares of these residuals as a smooth function of age, using GAMM. For male and female infants, the square root of the fit provided the estimate for the standard deviation of the spread in volume around the respective mean as a function of age. We then estimated volumes for various percentiles from the inverse of the corresponding normal cumulative distribution function (eMethods in the Supplement).

Results

Regional Brain Growth Trajectories

Spaghetti plots for male and female whole-brain sizes are shown in Figure 2A, along with GAMM fits to the Equation for the growth trajectories. The estimated intercepts (sizes at birth) are 347 cm^3 for male and 335 cm^3 for female infants (for the results obtained when controlling for head circumference or body length at birth, see eResults, eFigures 2 and 3, and eTables 2 and 3 in the Supplement). Numerical values for all ROIs are listed in Table 2, with spaghetti plots in eFigures 4 and 5 in the Supplement. As expected, gestational age at birth (g_0 coefficients) did have a significant effect on structure size for all ROIs, except the pallidum and third ventricle, with longer gestation leading to larger size at birth. In addition, there was a significant interaction between gestational age at birth and age (g_t = −8.334 mm^3/d^2; SE, 3.202; P = .010), indicating “catching up” among those born earlier than average. By 90 days after birth, male brains had grown more rapidly (66%) than female brains (63%); the highest growth rates were found for the cerebellum: 113% in male and 105% in female infants. Values for other ROIs are in Table 3. Volume-by-age percentile plots are shown in Figure 2C and 2D for whole brain and in eFigure 6 in the Supplement for caudate, cerebellum, putamen, and lateral ventricles. When an infant’s head circumference or body length and/or gestational age at birth is known, the residualized volume-for-age percentile plots (eFigure 3 in the Supplement) can be used, with substantially narrower variance.

Adult whole-brain volume, estimated from the Alzheimer Disease Neuroimaging Initiative data (eMethods in the Supplement) averaged across the sexes, was 1018 cm^3 (minimum, 802 cm^3; maximum, 1263 cm^3; SD, 99 cm^3). The estimated mean whole-brain volume in the current study was 341 cm^3 at birth and 558 cm^3 at 90 days. Therefore, on average, the brains of neonates grew from 33.5% to 54.9% of adult brain size between birth and 90 days.

Sexual Dimorphism

In the full data set, sex did not affect cerebral structure size at birth (though there was a significant difference between male and female infants in the subset of 63 subjects with controlling for body length or head circumference at birth; eTable 2 in the Supplement). However, there was a significant sex × age effect for the whole brain, ventricles, and putamen, with a trend toward significance for the cerebellum, leading to larger structure sizes with advancing age for male relative to female infants (see s_t coefficients in Table 2).

Left-Right Asymmetry

We also evaluated left and right volume difference for all bilateral ROIs. Results for the lateral ventricles are shown in eFigure 7 in the Supplement. During the first 3 months of postnatal life, the left ventricle is significantly larger than the right by 462 mm^3 (approximately 5% of the size of a lateral ventricle at 2 months; SE, 38 mm^3; $P < 10^{-16}$). Values for all ROIs are shown in Table 3 (eFigure 8 in the Supplement).

Rates of Change in Growth Trajectories

An estimate of the rate of growth for the whole brain as a function of age, expressed as a percentage of the structure size at that age, is shown in Figure 2B, which displays both a GAMM fit based on the strictly longitudinal data, controlling for gestational age at birth and sex, and the gradient of the growth trajectory fit to all the data. The pronounced features of these plots are very high initial rate of growth, approximately 1%/d, and decreasing rate of growth during the subsequent months, with indications of tapering off to 0.4%/d near 3 months of age. Plots for the other ROIs examined are shown in eFigures 4 and 5 in the Supplement.

Discussion

To our knowledge, early brain development in healthy term-born or term-equivalent preterm-born infants has not previously been extensively studied, leaving considerable gaps in knowledge of this crucial developmental period. Using longitudinal analysis of MR images, we found that brain development in neonates is most rapid in the days immediately after birth, when whole-brain growth rate initially is approximately 1%/d, slowing to 0.4%/d by the end of the first 3 months, with overall growth of 64% in 90 days. Consistent with this rapid growth, we found that longer gestation led to larger brain size at birth. Male infants showed greater increase in whole-brain volume over time, although this difference at birth was significant only when we controlled for head circumference or body length at birth. The cerebellum grew at the highest rate, more than doubling in volume in 90 days, while the hippo-campus grew at the slowest rate, increasing in volume by only 47% in 90 days. As with the whole brain, the growth rate for all ROIs decreased substantially during the first 3

months. We found left-right asymmetry in multiple ROIs, particularly the lateral ventricles where the left was larger than the right by 462 mm^3 on average (about 5% of lateral ventricle volume at 2 months). The left caudate and amygdala were also larger than the right. However, the right hippocampus, thalamus, putamen, and cerebellum were larger than the left. Finally, we calculated volume-by-age percentile plots for the whole brain and for multiple ROIs, which may be useful for assessing individual brain development or response to therapy.

Regional volume increases in the human brain during the first 3 months after birth arise from multiple factors, including postnatal migration of neurons from the ventricular (or proliferative) zone, with total numbers of cortical neurons increasing by 23%–30% from birth to age 3 months[26]; synaptogenesis and proliferation; dendritic and axonal growth along with increased neuropil arborization; differentiation and proliferation of glia; and subcortical white matter myelination by oligodendrocytes.[27,28] These processes occur in tandem with the competing processes of synaptic pruning and apoptosis[28,29] that tend to reduce volume. Differences in regional growth rates during infancy probably reflect relative differences in developmental processes at this stage. For example, we found that the cerebellum—which constitutes 6.5% of the total volume of the brain at birth yet contains more than half of its neurons—undergoes the highest rate of growth during the first 3 months after birth, in agreement with findings of a cross-sectional study during the first 2 years of life,[18] which may reflect the importance of early development of motor control. In contrast, the hippocampus is the most slowly growing region during the first 3 months, which suggests that the development of episodic or autobiographical memory is not a key process at this stage of life.

Our finding of larger left than right lateral ventricle is in agreement with an earlier in utero ultrasound study[30] and cross-sectional studies of neonates.[6,31] The asymmetries for the amygdala and thalamus are consistent with recent findings in adolescents,[32] suggesting that the adolescent-stage asymmetry for each of these ROIs is already established in the neonatal period. Moreover, the hippocampal asymmetry is consistent with cross-sectional studies in neonates[33] and in children and adolescents.[34,35] It has been suggested that this asymmetry arises in the early adolescent years.[32] Our results, however, indicate that it already occurs in the early postnatal period. Cerebral asymmetry has been associated with asymmetric or lateralized functional specializations seen in adults, including handedness, dexterity, and language abilities,[36] and although little is known about the origins of anatomical and functional asymmetries in the brain[37] they are thought to arise from asymmetric gene expression in the embryonic human cortex.[38] In addition, several neurological disorders are believed to be developmental and are associated with atypical brain asymmetry,[39] particularly schizophrenia[40] and autism.[41] Thus, early deviant brain asymmetry—which may be opposite from later brain asymmetry[42]—may provide an index for individuals being at risk for a neurodevelopmental disorder.

A limitation of this study is that longitudinal tissue contrast change was not explicitly modeled. Furthermore, depending on age, certain neighboring ROIs can appear similar on T1 and/or T2 images; for example, the caudate or thalamus may show similar intensity as the adjacent cerebral white matter. This problem might be ameliorated by use of additional

MRI sequences, such as magnetization transfer imaging or diffusion tensor imaging. In cases of similar contrast, however, the boundary between ROIs may remain uncertain, and its location will be determined primarily from morphometric mapping of spatial priors derived from manual segmentation.

For the ROIs examined, the whole brain was the best delineated on T1-weighted and T2-weighted MR images, leading to the most accurate segmentation, followed by the cerebellum, thalamus, caudate, putamen, lateral ventricles, and hippocampus. However, other smaller structures—the pallidum, amygdala, and fourth ventricle—were least well defined. Resolution in the MR images was insufficient to accurately delineate the very thin early postnatal cortex, compounded by the poor contrast-to-noise ratio between the developing gray matter and largely unmyelinated white matter. Thus, we did not examine cortical development. The quality of many images was less than optimal owing to subject motion, a problem that could be mitigated by using prospective motion correction techniques.[43–45] With more images of higher quality, greater precision in ROI segmentation can be expected. Another source of error in growth trajectories comes from the inherent uncertainty in determining gestational age[25]: due to rapid growth, 1 week is a long time in fetal and neonatal development, and many gestational ages at birth were reported in whole-week units.

Conclusions

Despite these limitations, we accurately mapped out early postnatal whole-brain growth trajectories for male and female infants, which, to our knowledge, has not been done, and we provided the first estimates for growth trajectories of subcortical areas during the first 3 months after birth. Establishing normative data like these on larger and more diverse or representative samples, particularly volume-by-age percentile plots, could provide a valuable reference for assessing cerebral development and monitoring effects of intervention on brain growth in any infants with perinatal insults, during the most dynamic postnatal growth phase for the human brain. Regional growth rates and left-right asymmetries should also inform a deeper understanding of the relationship between brain structure and function when both are developing rapidly and may provide an early indicator for abnormal brain development or future neuropsychiatric disorders.

Supplementary Material

Refer to Web version on PubMed Central for supplementary material.

Acknowledgments

Funding/Support: This study was supported by grants from the National Institutes of Neurological Disorders and Stroke (U54 NS056883), the National Institute on Drug Abuse (2K24-DA16170 and RC2-DA029475), and the National Institute on Minority Health and Health Disparities (G12-MD007601-26).

Role of the Sponsors: The funding sources had no role in the design and conduct of the study; collection, management, analysis, or interpretation of the data; preparation, review, or approval of the manuscript; and decision to submit the manuscript for publication.

References

1. Woodward LJ, Anderson PJ, Austin NC, Howard K, Inder TE. Neonatal MRI to predict neurodevelopmental outcomes in preterm infants. N Engl J Med. 2006; 355(7):685–694. [PubMed: 16914704]
2. Nossin-Manor R, Card D, Morris D, et al. Quantitative MRI in the very preterm brain: assessing tissue organization and myelination using magnetization transfer, diffusion tensor and T_1 imaging. Neuroimage. 2013; 64:505–516. [PubMed: 22982360]
3. Inder TE, Wells SJ, Mogridge NB, Spencer C, Volpe JJ. Defining the nature of the cerebral abnormalities in the premature infant: a qualitative magnetic resonance imaging study. J Pediatr. 2003; 143(2):171–179. [PubMed: 12970628]
4. Counsell SJ, Maalouf EF, Fletcher AM, et al. MR imaging assessment of myelination in the very preterm brain. AJNR Am J Neuroradiol. 2002; 23(5):872–881. [PubMed: 12006296]
5. Stiles J, Jernigan TL. The basics of brain development. Neuropsychol Rev. 2010; 20(4):327–348. [PubMed: 21042938]
6. Gilmore JH, Lin W, Prastawa MW, et al. Regional gray matter growth, sexual dimorphism, and cerebral asymmetry in the neonatal brain. J Neurosci. 2007; 27(6):1255–1260. [PubMed: 17287499]
7. C TE Jr. The circumference of the head of newborn infants first measured in 1785. Pediatrics. 1967; 39(6):883.
8. Daymont C, Hwang WT, Feudtner C, Rubin D. Head-circumference distribution in a large primary care network differs from CDC and WHO curves. Pediatrics. 2010; 126(4):e836–e842. [PubMed: 20855391]
9. Clinical Growth Charts. Centers for Disease Control and Prevention/National Center for Health Statistics. 2009. http://www.cdc.gov/growthcharts/clinical_charts.htm. Accessed April 14, 2014.
10. Child Growth Standards WHO. Methods and development Head circumference-for-age, arm circumference-for-age, triceps skinfold-for-age and subscapular skinfold-for-age: World Health Organization. 2007. http://www.who.int/childgrowth/publications/technical_report_2/en/. Accessed April 14, 2014.
11. Robertson RL, Robson CD, Zurakowski D, Antiles S, Strauss K, Mulkern RV. CT versus MR in neonatal brain imaging at term. Pediatr Radiol. 2003; 33(7):442–449. [PubMed: 12743660]
12. Brenner D, Elliston C, Hall E, Berdon W. Estimated risks of radiation-induced fatal cancer from pediatric CT. AJR Am J Roentgenol. 2001; 176(2):289–296. [PubMed: 11159059]
13. Sled JG, Nossin-Manor R. Quantitative MRI for studying neonatal brain development. Neuroradiology. 2013; 55(suppl 2):97–104. [PubMed: 23872867]
14. Williams LA, Gelman N, Picot PA, et al. Neonatal brain: regional variability of in vivo MR imaging relaxation rates at 3.0 T—initial experience. Radiology. 2005; 235(2):595–603. [PubMed: 15858099]
15. Pienaar R, Fischl B, Caviness V, Makris N, Grant PE. A methodology for analyzing curvature in the developing brain from preterm to adult. Int J Imaging Syst Technol. 2008; 18(1):42–68. [PubMed: 19936261]
16. van der Knaap MS, van Wezel-Meijler G, Barth PG, Barkhof F, Adèr HJ, Valk J. Normal gyration and sulcation in preterm and term neonates: appearance on MR images. Radiology. 1996; 200(2): 389–396. [PubMed: 8685331]
17. Gilmore JH, Shi F, Woolson SL, et al. Longitudinal development of cortical and subcortical gray matter from birth to 2 years. Cereb Cortex. 2012; 22(11):2478–2485. [PubMed: 22109543]
18. Knickmeyer RC, Gouttard S, Kang C, et al. A structural MRI study of human brain development from birth to 2 years. J Neurosci. 2008; 28(47):12176–12182. [PubMed: 19020011]
19. Wang L, Shi F, Li G, et al. Segmentation of neonatal brain MR images using patch-driven level sets. Neuroimage. 2014; 84:141–158. [PubMed: 23968736]
20. Wang L, Shi F, Gao Y, et al. Integration of sparse multi-modality representation and anatomical constraint for isointense infant brain MR image segmentation. Neuroimage. 2014; 89:152–164. [PubMed: 24291615]

21. Wang L, Shi F, Yap PT, Gilmore JH, Lin W, Shen D. 4D multi-modality tissue segmentation of serial infant images. PLoS One. 2012; 7(9):e44596. [PubMed: 23049751]
22. Holland D, Dale AM, Alzheimer's Disease Neuroimaging Initiative. Nonlinear registration of longitudinal images and measurement of change in regions of interest. Med Image Anal. 2011; 15(4):489–497. [PubMed: 21388857]
23. Holland D, McEvoy LK, Dale AM, Alzheimer's Disease Neuroimaging Initiative. Unbiased comparison of sample size estimates from longitudinal structural measures in ADNI. Hum Brain Mapp. 2012; 33(11):2586–2602. [PubMed: 21830259]
24. Wood SN. Low-rank scale-invariant tensor product smooths for generalized additive mixed models. Biometrics. 2006; 62(4):1025–1036. [PubMed: 17156276]
25. Engle WA, American Academy of Pediatrics Committee on Fetus and Newborn. Age terminology during the perinatal period. Pediatrics. 2004; 114(5):1362–1364. [PubMed: 15520122]
26. Shankle WR, Rafii MS, Landing BH, Fallon JH. Approximate doubling of numbers of neurons in postnatal human cerebral cortex and in 35 specific cytoarchitectural areas from birth to 72 months. Pediatr Dev Pathol. 1999; 2(3):244–259. [PubMed: 10191348]
27. Huttenlocher PR, Dabholkar AS. Regional differences in synaptogenesis in human cerebral cortex. J Comp Neurol. 1997; 387(2):167–178. [PubMed: 9336221]
28. Lenroot RK, Giedd JN. Brain development in children and adolescents: insights from anatomical magnetic resonance imaging. Neurosci Biobehav Rev. 2006; 30(6):718–729. [PubMed: 16887188]
29. Marsh R, Gerber AJ, Peterson BS. Neuroimaging studies of normal brain development and their relevance for understanding childhood neuropsychiatric disorders. J Am Acad Child Adolesc Psychiatry. 2008; 47(11):1233–1251. [PubMed: 18833009]
30. Achiron R, Yagel S, Rotstein Z, Inbar O, Mashiach S, Lipitz S. Cerebral lateral ventricular asymmetry: is this a normal ultrasonographic finding in the fetal brain? Obstet Gynecol. 1997; 89(2):233–237. [PubMed: 9015026]
31. Ichihashi K, Iino M, Eguchi Y, Uchida A, Honma Y, Momoi M. Difference between left and right lateral ventricular sizes in neonates. Early Human Development. 2002; 68(1):55–64. [PubMed: 12191529]
32. Dennison M, Whittle S, Yücel M, et al. Mapping subcortical brain maturation during adolescence: evidence of hemisphere- and sex-specific longitudinal changes. Dev Sci. 2013; 16(5):772–791. [PubMed: 24033581]
33. Thompson DK, Wood SJ, Doyle LW, Warfield SK, Egan GF, Inder TE. MR-determined hippocampal asymmetry in full-term and preterm neonates. Hippocampus. 2009; 19(2):118–123. [PubMed: 18767066]
34. Giedd JN, Vaituzis AC, Hamburger SD, et al. Quantitative MRI of the temporal lobe, amygdala, and hippocampus in normal human development: ages 4–18 years. J Comp Neurol. 1996; 366(2): 223–230. [PubMed: 8698883]
35. Uematsu A, Matsui M, Tanaka C, et al. Developmental trajectories of amygdala and hippocampus from infancy to early adulthood in healthy individuals. PLoS One. 2012; 7(10):e46970. [PubMed: 23056545]
36. Ratnarajah N, Rifkin-Graboi A, Fortier MV, et al. Structural connectivity asymmetry in the neonatal brain. Neuroimage. 2013; 75:187–194. [PubMed: 23501049]
37. Bishop DV. Cerebral asymmetry and language development: cause, correlate, or consequence? Science. 2013; 340(6138):1230531. [PubMed: 23766329]
38. Sun T, Walsh CA. Molecular approaches to brain asymmetry and handedness. Nat Rev Neurosci. 2006; 7(8):655–662. [PubMed: 16858393]
39. Hendren RL, De Backer I, Pandina GJ. Review of neuroimaging studies of child and adolescent psychiatric disorders from the past 10 years. J Am Acad Child Adolesc Psychiatry. 2000; 39(7): 815–828. [PubMed: 10892223]
40. Oertel-Knöchel V, Linden DE. Cerebral asymmetry in schizophrenia. Neuroscientist. 2011; 17(5): 456–467. [PubMed: 21518811]
41. Herbert MR, Ziegler DA, Deutsch CK, et al. Brain asymmetries in autism and developmental language disorder: a nested whole-brain analysis. Brain. 2005; 128(pt 1):213–226. [PubMed: 15563515]

42. Shaw P, Greenstein D, Lerch J, et al. Intellectual ability and cortical development in children and adolescents. Nature. 2006; 440(7084):676–679. [PubMed: 16572172]

43. White N, Roddey C, Shankaranarayanan A, et al. PROMO: Real-time prospective motion correction in MRI using image-based tracking. Magn Reson Med. 2010; 63(1):91–105. [PubMed: 20027635]

44. Kuperman JM, Brown TT, Ahmadi ME, et al. Prospective motion correction improves diagnostic utility of pediatric MRI scans. Pediatr Radiol. 2011; 41(12):1578–1582. [PubMed: 21779892]

45. Brown TT, Kuperman JM, Erhart M, et al. Prospective motion correction of high-resolution magnetic resonance imaging data in children. Neuroimage. 2010; 53(1):139–145. [PubMed: 20542120]

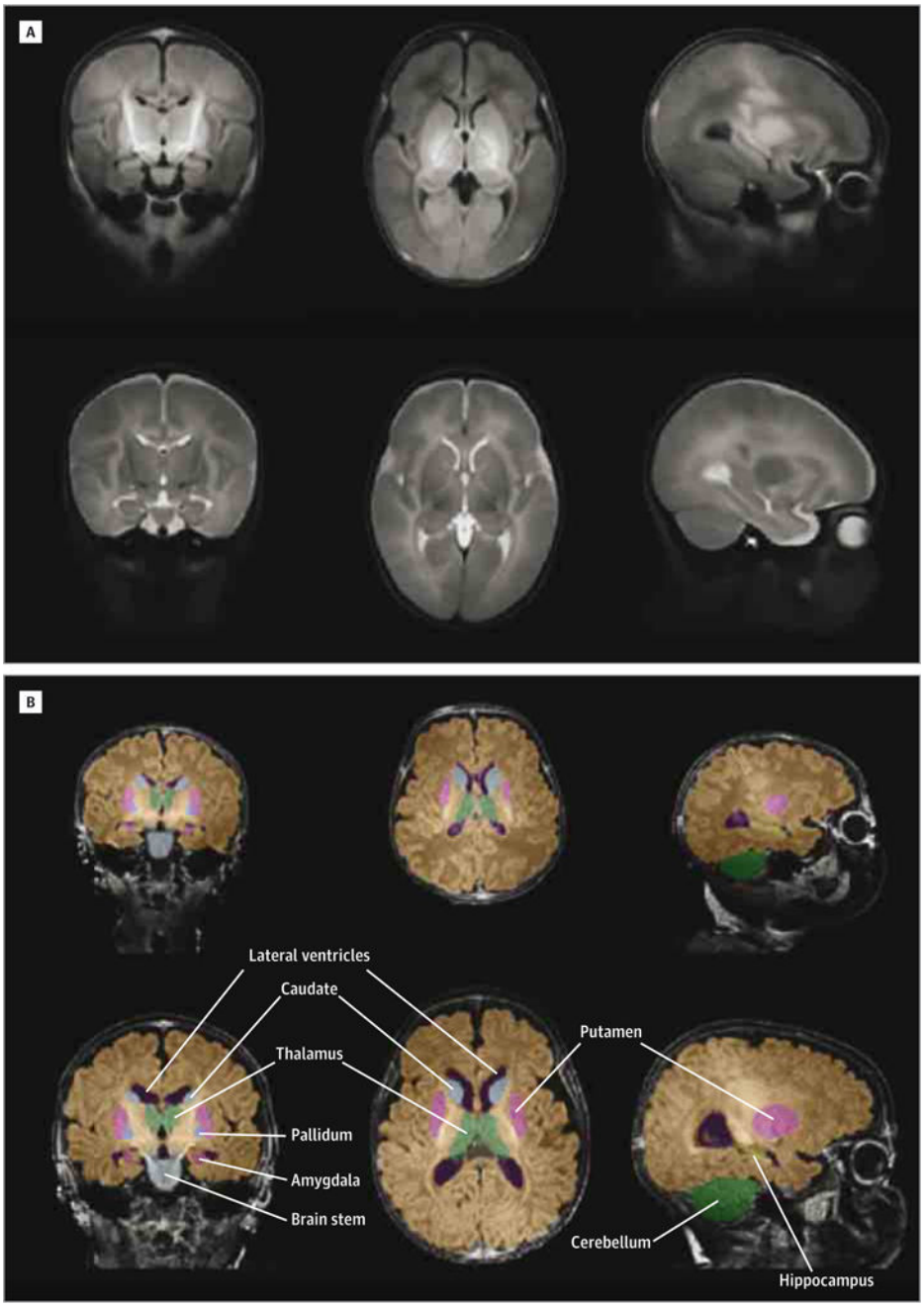

Figure 1. Infant Atlas and Automatically Segmented Magnetic Resonance Images

A, Cross-sections through T1 (upper) and T2 (lower) atlas images.

B, Examples of automatic segmentation. Upper row: 5-day-old male neonate (brain volume, 3.1×10^5 mm^3; 30% of elderly adult brain volume); lower row, 117-day-old male infant with a brain more than twice as large (brain volume, 6.6×10^5 mm^3; 65% of adult brain volume). Color key: yellow, hippocampus; pink, putamen; light blue, caudate; medium blue, pallidum; light green, thalamus; purple, ventricles; dark green, cerebellum; gray, brain stem; brown, rest of whole-brain parenchyma.

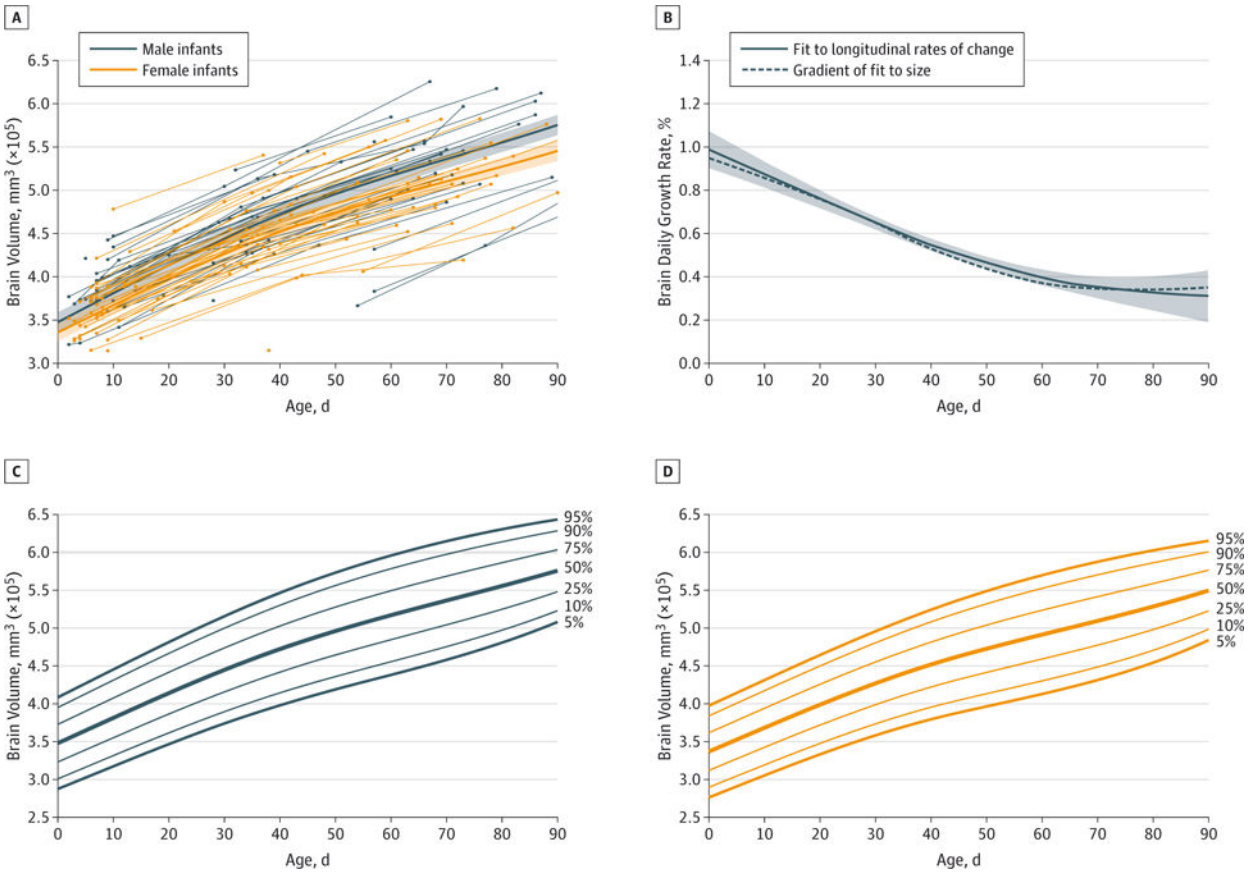

Figure 2. Whole-Brain Growth Trajectories, Daily Growth Rates, and Volume-for-Age Percentile Plots

A, Spaghetti plot showing whole-brain volume for 39 male and 48 female infants (94 and 117 time points, respectively) during the first 3 months of postnatal life, along with generalized additive mixed model (GAMM) fits to the data (dark lines, from the Equation), and 95% CIs (shaded regions); see also eFigure 2 in the Supplement. B, Daily growth rate for the whole brain during the first 3 months of postnatal life (for male and female infants combined). The dashed line is the gradient of a GAMM fit for whole-brain volume trajectory; the solid line is a GAMM fit to centered linear estimates of the growth rates (between each subject's neighboring data points) from the longitudinal data only. Whole-brain volume-by age percentile plots for boys (C) and girls (D) (see also eFigure 3B and 3D in the Supplement); these plots can be used when controlling for an infant's head circumference and gestational age at birth.

Table 1

Subject Characteristics at Birth and at Baseline Images

Characteristics	Mean (SE) Value[a]		*P* Value
	Male Infants (n = 39)[b]	Female Infants (n = 48)[c]	
Characteristics at birth			
Postmenstrual age, wk	38.5 (0.4)	38.8 (0.3)	.51
Weight, kg[d]	3.2 (0.1)	3.2 (0.1)	.90
Length, cm[e]	50.6 (0.5)	50.2 (0.4)	.58
Head circumference, cm[f]	34.1 (0.4)	34.3 (0.3)	.76
Birth by vaginal/cesarean delivery, No.[g]	26/11	29/13	.49
Apgar score			
At 1 min	7.6 (0.2)	8.0 (0.2)	.21
At 5 min	8.8 (0.1)	8.9 (0.1)	.20
Mother's age at delivery, y	28.2 (1.0)	30.1 (0.9)	.15
Maternal weight gain, kg	13.6 (0.9)	15.0 (1.3)	.36
Characteristics at baseline imaging			
Postmenstrual age, wk	40.8 (0.4)	40.5 (0.3)	.52
Weight, kg	3.6 (0.1)	3.5 (0.1)	.43
Length, cm	52.1 (0.5)	51.3 (0.4)	.19
Head circumference, cm	36.0 (0.3)	35.3 (0.2)	.07

[a] Data represent mean (SE) values except for delivery type.

[b] All 39 male infants had baseline images, and 29 had 1 follow-up image: 8 had just 1 follow-up image, 16 had 2, and 5 had 3 (total of 94 time points).

[c] All 48 female infants had baseline images, and 38 had 1 follow-up image; 10 had just 1 follow-up image, 25 had 2, and 3 had 3 (total of 117 time points).

[d] Birth weight was available for only 38 male and 47 female infants.

[e] Birth length was available for only 34 male and 46 female infants. The value for boys is similar to World Health Organization data[10] (WHO length, 49.88 cm; $P = .16$), but the value for girls is significantly higher (WHO length, 49.15 cm; $P = .01$).

[f] Head circumference at birth was available for only 30 male and 35 female infants. The values for both boys and girls are similar to WHO data[10] (boys, 34.46 cm [$P = .38$]; girls, 33.88 cm [$P = .17$]).

[g] Type of delivery was not known for 2 male and 6 female infants.

Table 2

Model Results for Growth Trajectories

	Gestational Age, mm^3/d^a			Gestation × Age, mm^3/d^{2a}			Sex × Age, mm^3/d^a		
Region of Interest	g_0	**SE**	***P* Value**	g_t	**SE**	***P* Value**	s_t	**SE**	***P* Value**
Whole brain[b]	**2215.2**	284.7	4×10^{-13}	**−8.334**	3.202	.010	**−200.4**	67.2	.003
Lateral ventricles	**47.0**	10.3	9×10^{-6}	**−0.330**	0.111	.0033	**−7.5**	3.8	.049
Ventricles	**37.6**	12.6	.0033	−0.013	0.172	.94	**−7.7**	3.8	.04
Cerebellum	**150.1**	34.7	2×10^{-5}	0.458	0.439	.30	−26.9	15.2	.08
Thalamus	**28.5**	5.4	4×10^{-7}	**−0.178**	0.082	.03	−0.5	2.0	.81
Caudate	**17.1**	3.3	6×10^{-7}	−0.048	0.045	.28	−0.4	1.1	.73
Putamen	**10.9**	2.2	1×10^{-6}	−0.024	0.024	.33	**−1.3**	0.5	.02
Pallidum	0.4	0.3	.12	0.007	0.004	.067	−0.1	0.1	.35
Ventricle									
Third	3.2	3.3	.34	−0.001	0.051	>.98	−2.1	1.3	.10
Fourth	**4.6**	0.7	5×10^{-10}	**−0.029**	0.007	3×10^{-5}	**−0.6**	0.2	.009
Brain stem	**21.2**	4.2	9×10^{-7}	0.009	0.050	.87	−1.1	1.7	.50
Hippocampus	**4.3**	0.8	1×10^{-7}	**−0.034**	0.011	.0027	−0.3	0.3	.21
Amygdala	**1.8**	0.3	4×10^{-8}	**−0.009**	0.004	.041	−0.1	0.1	.36

[a] In the notation of the Equation, the coefficients g_0 and g_t represent gestational age, and s_t represents sex; none of the *P* values for s_0 showed significance. For g_0, positive coefficients indicate larger structures at birth for older-than-average gestational age at birth; for g_t, negative coefficients indicate faster growth rate for those born earlier than average; and for s_t, negative coefficients indicate a widening gap with age between structure size in male and female infants, with smaller structures in female infants. As an example of the effect of gestational age, for a girl born 1 week earlier than average, the expected brain size will be 5% smaller than average at birth and 2% smaller than average at 90 days after birth. Bold values are significant at the α = .05 level (false-positive probability level of 5%).

[b] See also eTables 2 and 3 in the Supplement for values obtained when controlling for head circumference or body length at birth.

Table 3

Structure Sizes at Birth, Effective Rates of Growth Over 3 Months, and Mean Lateral Asymmetries

	Volume at Birth (Intercept), mm^3[a]					Growth After 90 Days, %	Left-Right Asymmetry	
Region of Interest	**Male Infants**	**SE**	**Female Infants**	**SE**	***P* value**	**Male/Female/All Infants**	**Mean (SE), mm^3[b]**	***P* value**
Whole brain[c]	34 7388	5753	33 5509	5105	.12	66/63/64	NA	NA
Lateral ventricles	5962	204	5741	182	.42	83/74/78	**462** (38)	$<10^{-16}$
Ventricles	7389	240	7061	212	.31	81/75/78	NA	NA
Cerebellum	22 793	624	22 337	560	.59	113/105/108	**−169** (54)	.002
Thalamus	4133	97	4072	85	.64	54/54/54	**−116** (12)	$<10^{-16}$
Caudate	2487	62	2395	54	.27	66/67/66	**28** (6)	3×10^{-6}
Putamen	2474	44	2417	39	.32	54/50/52	**−57** (5)	$<10^{-16}$
Pallidum	206	5	210	5	.59	58/53/55	−3 (2)	.14
Ventricle								
Third	877	61	866	53	.90	76/55/64	NA	NA
Fourth	416	14	417	13	.95	88/75/81	NA	NA
Brain stem	4109	75	4042	68	.51	65/63/64	NA	NA
Hippocampus	479	14	484	12	.81	50/44/47	**−22** (3)	1×10^{-13}
Amygdala	214	6	203	5	.16	58/57/58	**12** (1)	$<10^{-16}$

Abbreviation: NA, not applicable.

[a] In the notation of the Equation, s_0 = (female intercept) − (male intercept). Expressed as a percentage of female brain size, the male brain is larger than the female brain by 3.5% (95% CI, −0.9% to 8.0%) at birth and by 5.5% (95% CI, 2.5% to 8.5%) at 90 days after birth.

[b] Bold values are significant at the $\alpha = .05$ level.

[c] See also eTables 2 and 3 in the Supplement for values obtained when controlling for head circumference or body length at birth.